ACS OMEGA

http://pubs.acs.org/journal/acsodf

Article

Photophysical Properties of Naphthalene-oxacalix[*m*]arene and Recognition of Fullerene C_{60}

Yuming Yu,* Wei Lan, Xin Wang, Ming Gao, Rongrong Yang, Dou Wang, Shijun Sun, Yiran Wu, Yanfang Ma, Islam Siraj, Lang Liu, Duo-zhi Wang, Jianzhang Zhao, Xiaodong Cai, Hui Tan,* and Zhenjiang Liang*

Cite This: *ACS Omega* 2022, 7, 15411−15422

Read Online

ACCESS | Metrics & More | Article Recommendations | Supporting Information

ABSTRACT: Three different pore sizes of oxacalix[*m*]arene[*n*]pyrimidines modified with a naphthalene substituent were synthesized and characterized by HRMS, ^{1}H NMR, and single-crystal analysis (**8OA** and **8OA-N**). Steady-state spectroscopy indicates these naphthalene-oxacalix[*m*]arenes exhibit good fluorescence properties, which isattributed to the locally excited (LE) state emission, and electrochemical results show that the photoinduced electron transfer (PET) process occurs from the naphthalene substituent to the linked pyrimidine. Nanosecond transient absorption spectra, singlet oxygen quantum yields ($\Phi_{\Delta 4OA\text{-}N}$ = 45.1%, $\Phi_{\Delta 6OA\text{-}N}$ = 56.6%, and $\Phi_{\Delta 8OA\text{-}N}$ = 65.7%) and theoretical calculations demonstrate that the torsion angle between the donor (naphthalene) and the acceptor (pyrimidine) promotes intersystem crossing (ISC), and the lifetime of the triplet state reaches ca. 8 ms. Interestingly, all three host molecules (**4OA-N**, **6OA-N**, and **8OA-N**) showed a high affinity for fullerene C_{60}, and significant binding constants in the range of 4.10−6.68 × 10^4 M^{-1} were obtained by fluorescence titration; in contrast, previous reports indicated that the similar oxacalix[*m*]-arene[*n*]pyrimidine scaffold could not efficiently complex with C_{60}. In the frontier molecular orbital theory calculations of the supramolecular system of **4OA-N@C_{60}**, the HOMO is distributed on **4OA-N** and the LUMO is localized on fullerene. The calculation results further demonstrated that there are strong interactions between the host and the fullerene guest, which is consistent with the result of the experiments. The characteristic photophysical properties of these novel naphthyl-decorated oxacalix[*m*]arene[*n*]pyrimidines broaden their application field, and the stable host−guest system with fullerene can be applied to supramolecular chemistry.

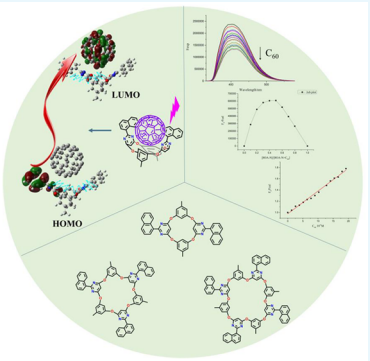

INTRODUCTION

Macrocyclic compounds play an important role in supramolecular chemistry. Their preconstructed rigid structures can effectively overcome the unfavorable factors caused by the reduction of entropy in molecular recognition and assembly. In recent years, heteroatom bridge and heteroaromatic hybrid calixarenes have widely attracted attention[1,2] and have been used in conformation control, molecular recognition, sensor systems, optoelectronic devices, and advanced materials.[3−10] According to previous reports, nitrogen as a bridging atom has different hybrid modes of sp^2, sp^3, or between them and can form different degrees of conjugation with adjacent aromatics, which means heterocalixarenes have adjustable configurations and the potential for application in supramolecular chemistry.[11] Additionally, there are similar properties when oxygen atoms act as bridging atoms. At present, there are many reports on the synthesis and modification of oxacalix[*m*]arenes[12−14] and a few reports about the application of oxacalix[*m*]arenes in supramolecular recognition. Wim Dehaen et al.[15] reported the presence of the anion receptors on the oxacalix[2]arene[2]-pyrimidine scaffold, and Chen et al.[16] reported that triptycene oxacalixarene derivatives were the hosts of fullerenes. Hitherto, the research on the host−guest chemistry of oxacalix[*m*]arenes is still insufficient, especially the introduction of specific luminescent substituents into supramolecular systems for energy or electron transfer.

Fullerenes (C_{60}) with unique structures and photoelectric properties have attracted much attention since their discovery in 1985.[17−20] Fullerenes can interact with the host molecules through the force of noncovalent bonds and are widely studied in the field of supramolecular chemistry.[21] The highly selective recognition of fullerenes through different hole sizes and geometries can not only separate and purify fullerene isomers but can also expand the application of fullerene-based materials and devices.[22−24]

Oxacalix[*m*]arenes are seldom applied in the assembly of host−guest system in supramolecular chemistry, especially

Received: December 14, 2021
Accepted: April 14, 2022
Published: April 27, 2022

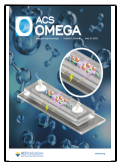

Scheme 1. Synthesis of the 4OA-N, 6OA-N, and 8OA-N

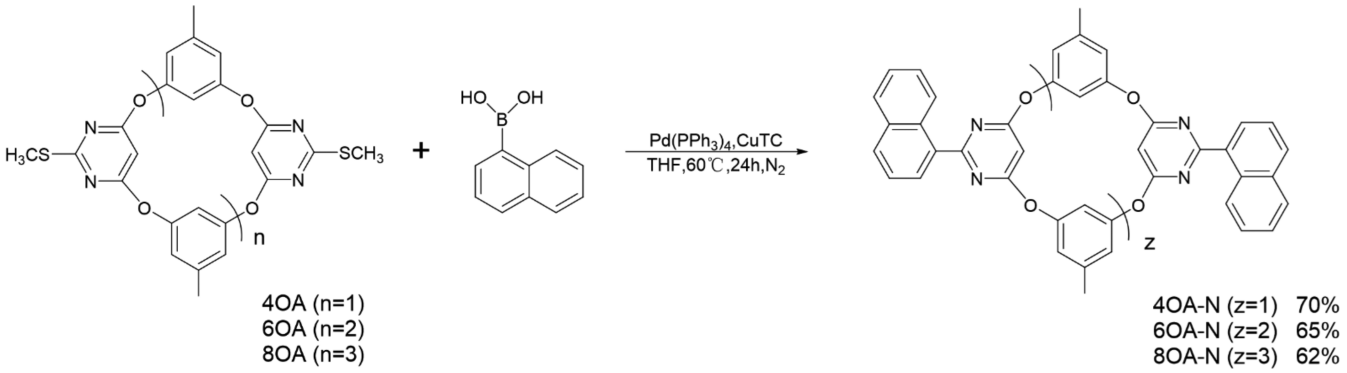

oxacalix[*m*]arenes hybridized with heteroaromatic rings.[25] Wim et al. reported that oxacalix[2]arene[2]pyrimidine-bis(Zn-porphyrin) selectively recognized C_{70}, and several other oxacalixrenes did not recognize C_{70} or C_{60}.[26] Therefore, we think that more oxacalixarenes should be synthesized and applied in supramolecular chemistry, particularly for interactions with fullerene C_{60}. Hence, we synthesized three oxacalix[*m*]arene[*n*]pyrimidine homologues **4OA**, **6OA**, and **8OA**[27] and modified them with a naphthyl group to give **4OA-N**, **6OA-N**, and **8OA-N**, respectively (Scheme 1 and Figures S1−S4). The photoproperties of the target oxacalix[*m*]arenes were tested using spectroscopic methods, and the three homologues show similar fluorescence emission behaviors. Interestingly, when the interactions between the host oxacalix[*m*]arene[*n*]pyrimidines and the guest fullerene C_{60} were measured in a toluene solution, they could form a stable concave-convex complex with a ratio of 1:1 and exhibited a high association constant. The study of oxacalix[*m*]arenes opens the way for the selective and efficient recognition of C_{60}, which could be applied to supramolecular chemistry.

EXPERIMENTAL SECTION

Materials and Methods. NMR spectra were acquired on commercial instruments (VARIAN INOVA-400 MHz). Chemical shifts (δ) are reported in parts per million (ppm) and referenced to the signals of tetramethylsilane or the internal (NMR) solvent. High-resolution mass spectra (HRMS) were recorded on a Bruker Daltonics Micro TOF-Q II spectrometer. UV−vis spectra were obtained on a U-3900H instrument. Fluorescence spectra and binding constants with fluorescence titration were acquired using an F-4500 spectrofluorometer. Nanosecond transient absorption spectra were recorded on an LP980 laser flash-photolysis spectrometer (Edinburgh Instrument Ltd., UK) equipped with an OPO laser (Opolette, the wavelength is tunable in the range of 210−2400 nm; OPOTEK, U.S.); the typical laser energy was ca. 5 mJ per pulse. The data (kinetic decay curve and spectrum) were obtained with the L900 software. Chemicals received from commercial sources were used without further purification. K_2CO_3 (anhydrous, granulated) was finely ground (with mortar and pestle) prior to use. Reaction solvents (DMF, petroleum ether, ethyl acetate, THF, and CH_2Cl_2; ≥99.5%) were used as received from commercial sources and not dried further prior to use.

Calculations. Density functional theory (DFT) calculations were used to optimize the ground-state geometries at the B3LYP/6-31G level. All the calculations were performed with Gaussian 09.

Lippert−Mataga equation. The simplest consideration for the general solvent effect is the Lippert−Mataga equation, which assumes that same excited -state is involved in both absorption and emission and that the energy difference between the ground state and the excited state is only proportional to solvent orientation polarizability ($\triangle f$).

$$\triangle\nu = \frac{2\triangle f}{4\pi\varepsilon_0 hca^3}(\mu_e - \mu_g)^2 + \text{constant} \quad (1)$$

$$\triangle f = \frac{\varepsilon - 1}{2\varepsilon + 1} + \frac{n^2 - 1}{2n^2 + 1} \quad (2)$$

where $\triangle\nu = \nu_{abs} - \nu_{em}$ stands for the Stokes shift (ν_{abs} and ν_{em} are the absorption and emission (cm^{-1}), respectively), h is Planck's constant, c is the velocity of light in a vacuum, a is the radius of the solvent cavity in which the fluorophore resides (the Onsager cavity radius), $\triangle f$ is the orientation polarizability, μ_g and μ_e are the ground-state dipole in the ground-state geometry and the excited dipole in the excited-state geometry, respectively, ε is the permittivity of the vacuum, and n is the refractive index.

Singlet Oxygen Quantum Yield. The singlet oxygen of the photosensitizer was measured using a 355 nm excitation lamp source and 1,3-diphenylisobenzofuran (DPBF) as an $^1O_2$ scavenger. The $^1O_2$ production was monitored by following the absorbance of DPBF at 414 nm. To determine the singlet oxygen quantum yield (Φ_Δ), a relative method was used according to eq 3. $Ru(bpy)_3[PF_6]_2$ was used as the standard (Φ_{std} = 0.57 in dichloromethane).

$$\Phi_{sam} = \Phi_{std}\left(\frac{1 - 10^{-A_{std}}}{1 - 10^{-A_{sam}}}\right)\left(\frac{m_{sam}}{m_{std}}\right)\left(\frac{\eta_{sam}}{\eta_{sam}}\right)^2 \quad (3)$$

In the above equation, "sam" and "std" represent the sample and the standard, respectively. Φ, A, m, and η represent the singlet oxygen quantum yield, the absorbance at the excitation wavelength, the change in the slope of the absorbance of DPBF over time, and the refractive index of the solvent used for measurement, respectively.

RESULTS AND DISCUSSION

Synthesis and Characterization. The synthesis of **4OA-N**, **6OA-N**, and **8OA-N** is shown in Scheme 1. A convenient one-pot procedure for the synthesis of oxacalix[*m*]arene[*n*]-pyrimidine was developed in a previous work, and we

https://doi.org/10.1021/acsomega.1c07068
ACS Omega 2022, 7, 15411−15422

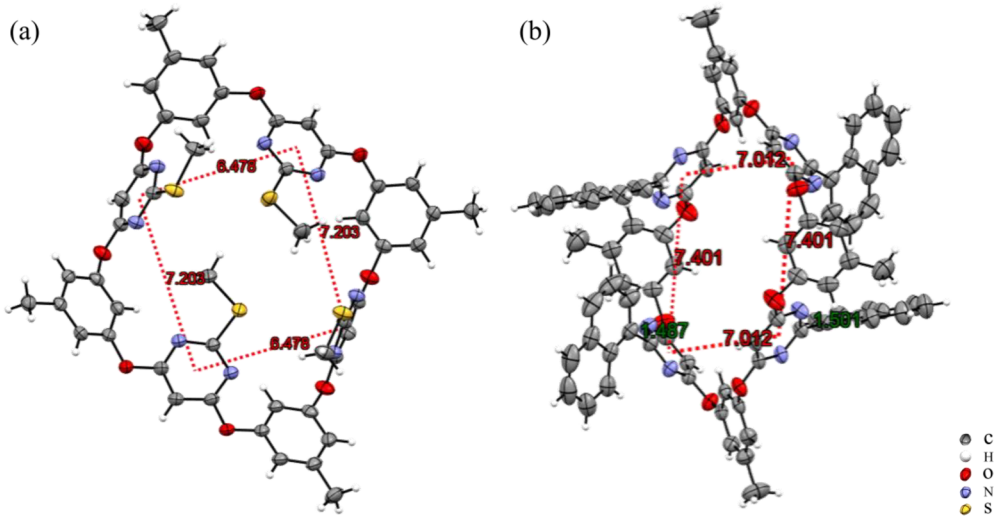

Figure 1. The crystal structures of (a) **8OA** and (b) **8OA-N**. The red dashed lines represent the distance between adjacent pyrimidine carbons, and the black dashed lines represent the bond length between naphthalene and the linked pyrimidine.

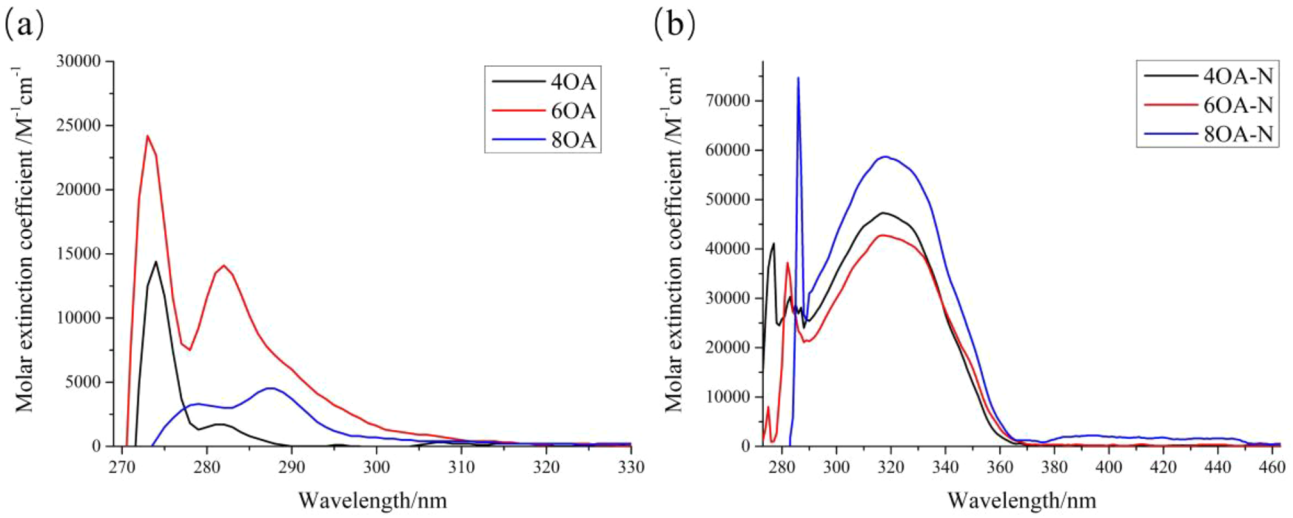

Figure 2. (a) UV−vis absorption spectra of **4OA**, **6OA**, and **8OA**. (b) UV−vis absorption spectra of **4OA-N**, **6OA-N**, and **8OA-N** in toluene (c = 1.0×10^{-5} M, 25 °C).

synthesized three precursors **4OA**, **6OA**, and **8OA** using this method.[28] Then, target compounds **4OA-N**, **6OA-N**, and **8OA-N** were obtained through a Liebeskind−Srögl coupling reaction[29,30] between the precursors and 1-naphthalene boric acid under N_2. **4OA-N**, **6OA-N**, and **8OA-N** were characterized by ^{1}H NMR spectroscopy and HRMS and further confirmed by single-crystal X-ray diffraction analysis.

Crystallographic Data of 8OA and 8OA-N. Diffraction-grade single crystals of **8OA** (CCDC 2070449) and **8OA-N** (CCDC 2070448) were obtained for the slow evaporation of a CH_2Cl_2/EtOAc solution. Crystal structures are shown in Figure 1a and b, and crystal data are shown in Tables S1 and S2. The distances between the naphthalene and the pyrimidine in **8OA-N** vary between 1.487 and 1.501 Å. This indicates that the molecular orbitals of naphthalene and pyrimidine overlap, resulting in a significant decrease in the C−C spacing. In **8OA** and **8OA-N**, the distance between adjacent pyrimidines is 6.476 and 7.203 Å and 7.012 and 7.401 Å respectively, which means that the pore size of **8OA-N** increases after the addition of the naphthalene substituents and the crystal density decreases (Figure S5c and d). These structural features are attributed to the charge distribution changes and spatial repulsion effects caused by the introduction of naphthyl groups.

As shown in Figure S5a and b, the intermolecular distance in **8OA** is 3.640 Å and that in **8OA-N** is 3.661 Å (red dashed line), respectively; both distances are less than 3.800 Å, showing the existence of intermolecular $\pi-\pi$ interactions.[31] Moreover, the shortest C−H···O distances in **8OA** and **8OA-N** are 2.919 and 2.943 Å (green dashed line), respectively, showing formation of intermolecular hydrogen bonding.[32] As shown in Figure S5b, the distances between naphthalene units and the adjacent pyrimidine are 7.102 and 7.815 Å within **8OA-N** (blue dashed line), indicating that there is no intramolecular interaction between naphthalene and the adjacent pyrimidine.

^{1}H NMR Analysis. In $CDCl_3$ and DMSO-d_6, **8OA** and **8OA-N** give rise to well-resolved ^{1}H NMR spectra, as shown in Figures S8 and S11, respectively. For instance, the single peaks at 2.26 and 3.39 ppm represent the methyl groups on benzene

https://doi.org/10.1021/acsomega.1c07068
ACS Omega 2022, 7, 15411−15422

Table 1. Photophysical properties of 4OA, 6OA, 8OA, 4OA-N, 6OA-N, and 8OA-N

compd	λ_{ex}[a] (nm) sol[e]	ε[b]	λ_{em}[c] (nm) sol[e]	Φ[d] (%) sol[e]	τ_F[e] (ns)	$\Phi_\triangle$[g] (%)
4OA	274/282	0.17	295	–[f]	–[f]	–[f]
6OA	273/282	1.41	294	–[f]	–[f]	–[f]
8OA	279/288	0.45	293	–[f]	–[f]	–[f]
4OA-N	277/317	4.72	384	27.50	1.0252 (96.78%) 19.0925 (3.22%)	45.10
6OA-N	282/317	4.28	414	28.93	1.1733 (31.15%) 7.9397 (68.49%)	56.60
80A-N	286/318	5.87	405	24.31	1.0732 (41.17%) 8.2853(58.82%)	65.70

[a]Absorption wavelength. [b]Molar extinction coefficient, $\varepsilon = 10^4$ M^{-1} cm^{-1}. [c]Emission wavelength. [d]Fluorescence quantum yield acquired using a calibrated integrating sphere. [e]In toluene. [f]Not applicable or not observed. [g]Singlet oxygen quantum yields. $Ru(bpy)_3[PF_6]_2$ was used as a standard compound ($\Phi_\triangle$ = 57% in DCM)

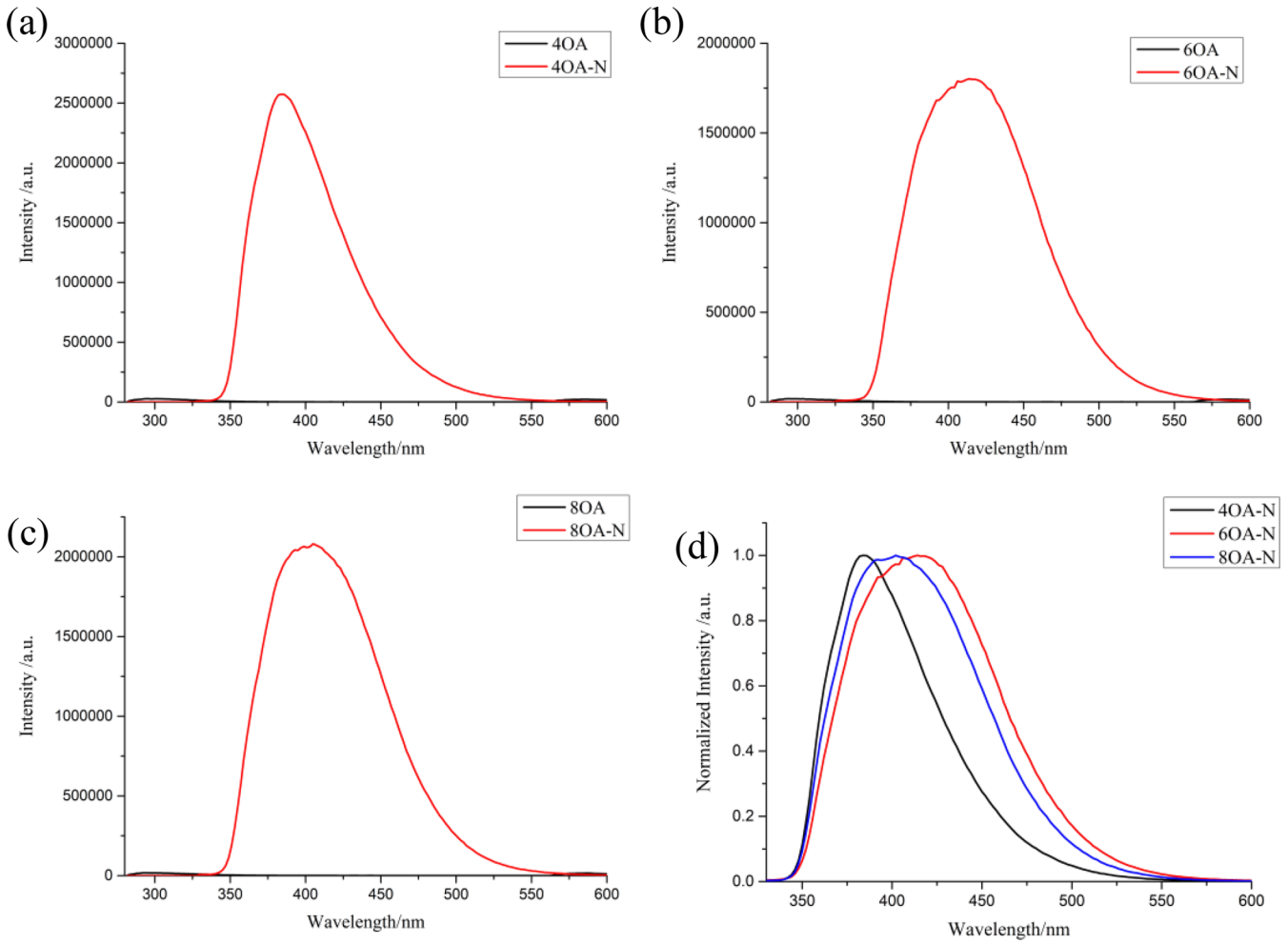

Figure 3. Fluorescence spectra of (a) **4OA** and **4OA-N**; (b) **6OA** and **6OA-N**; (c) **8OA** and **8OA-N**; and (d) **4OA-N**, **6OA-N**, and **8OA-N** normalized in toluene (c = 1.0 × 10^{-5} M, 25 °C).

and methyl groups with sulfur, respectively. After **8OA** was coupled with naphthyl, the peak of the methyl groups with sulfur disappeared and the signal of the naphthyl groups appeared in range of 7.20−8.60 ppm, indicating that the target molecules were prepared successfully.

UV−vis Absorption and Fluorescence Emission Spectra. Figure 2 and Table 1 are the UV−vis absorption spectra and photophysical parameters, respectively, of **4OA**, **6OA**, **8OA**, **4OA-N**, **6OA-N**, and **8OA-N**. **8OA** and **8OA-N** show absorption bands at 288 and 318 nm respectively, and the molar extinction coefficient (ε) of **8OA-N** ($\varepsilon_{318\ nm}$= 5.87 × 10^4 M^{-1} cm^{-1}) is over 13× that of **8OA** ($\varepsilon_{288\ nm}$= 0.45 × 10^4 M^{-1} cm^{-1}). After the introduction of the naphthyl group, the absorption band of **8OA-N** is obviously red-shifted compared with that of **8OA** (Figure S14). This could be attributed to the introduction of naphthyl as an electron-donating group reducing the HOMO and LUMO energy levels, which was also verified by theoretical calculations (Figure 8a).

The luminescent emission spectra of **4OA**, **6OA**, **8OA**, **4OA-N**, **6OA-N**, and **8OA-N** in toluene are shown in Figure 3a−c. **4OA**, **6OA**, and **8OA** have little fluorescence compared with **4OA-N**, **6OA-N**, and **8OA-N**. The maximum emission

https://doi.org/10.1021/acsomega.1c07068
ACS Omega 2022, 7, 15411−15422

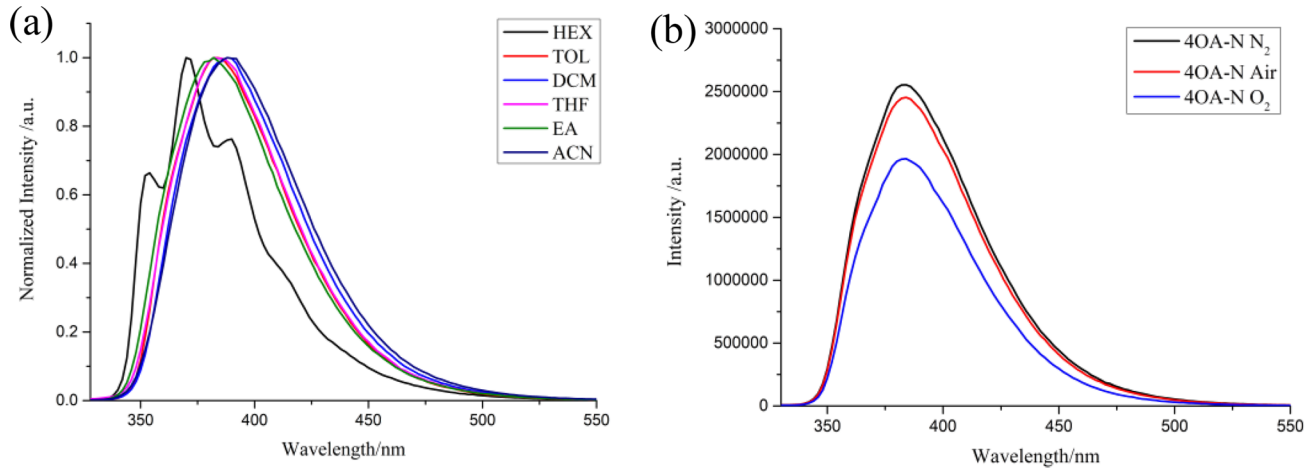

Figure 4. Fluorescence spectra of **4OA-N** in (a) different solvents and (b) a toluene solution under different atmospheres ($c = 1.0 \times 10^{-5}$ M, 25 °C).

wavelengths of **4OA-N**, **6OA-N**, and **8OA-N** are 384, 414, and 405 nm in toluene and the quantum yields are 27.50%, 28.93%, and 24.31%, respectively. Moreover, all three compounds exhibit similar emission behaviors (Figures 3d and S15d). In previous reports,[33,34] donor−acceptor (D−A) systems showed dual-fluorescence emission behavior, and the charge-transfer (CT) emission peak usually had bandwidth emission and an obvious red-shift relative to the maximum emission peak. In these naphthalene-oxacalix[*m*]arene analogues, there was no obvious shift in the emission peak of **4OA-N** with the increase in the solvent polarity, and **4OA-N** in the hexane solution exhibited a fine structure at 300−500 nm, which is characteristic of typical locally excited (LE) luminescence (Figure 4a).[35] To further assign the emission of the naphthalene-oxacalix[*m*]arene, the relationship between the Stokes shift $\triangle\nu$ and the polarity of the solvent $\triangle f$ was analyzed using the Lippert−Mataga equation.[36,37] The Lippert−Mataga diagrams are shown in Figures S16−S21, and the data are summarized in Tables S3−S8. The slope of the approximate line prepared from the emission band near 380 nm was almost zero. These data indicate that the luminescent bands around 380 nm should be assigned to the LE states of **4OA-N**, **6OA-N**, and **8OA-N**.

The fluorescence emission of **4OA-N** under the oxygen environment is lower than that under the nitrogen environment and is blue-shifted (Figures 4b, S22, and S23). The triplet levels (from theoretical calculations) of the three dyes ($E_{4OA\text{-}N,T1}$ = 1.90 eV, $E_{6OA\text{-}N,T1}$ = 1.91 eV, and $E_{8OA\text{-}N,T1}$ = 1.88 eV) are lower than the spectral levels in nitrogen and air environments ($E = 1240/\lambda_{em}$). We believe that this change in the luminescence intensity is not due to phosphorus emission.

Fullerene Binding Studies. At present, C_{60} has been developed as an electron receptor in host−guest systems.[38] Wang et al. designed and synthesized *N*-calixarenes that performed well in the subject−object recognition of C_{60} due to their unique pore cavity structure.[39] Here, the interaction of *O*-calixarenes with fullerene C_{60} was investigated by means of fluorescence titration experiments (Figures S24−S26). We found that the three congeners complex well with fullerene C_{60} in toluene solutions. The complexation constants range from 4.10×10^4 to 6.68×10^4 M^{-1}, and the complexation ratio is 1:1 (Table 2), indicating that the prepared *O*-calixarenes can effectively form stable host−guest complexes with C_{60}. The

Table 2. Complexation Parameters of 4OA-N, 6OA-N, and 8OA-N with C_{60} in a Toluene Solution at 298 K

compd	complexation constant (M^{-1})	complexation ratio
4OA-N	5.65×10^4	1:1
6OA-N	6.68×10^4	1:1
8OA-N	4.10×10^4	1:1

complexation constants have the order of magnitude but are not proportional to the pore sizes of the *O*-calixarenes, and the binding ability to C_{60} follows the order **6OA-N** > **4OA-N** > **8OA-N**. This indicates that the pore sizes of the *O*-calixarenes have effects on the capture of C_{60}.

The UV−vis absorption intensities of the three compounds increase with the concentration in accordance with the Lambert−Beer law (Figures 5a, S27, and S28). The UV−vis absorption spectra obviously changed after the addition of C_{60}, and isosbestic point for **8OA-N@C_{60}** was at 316 nm (Figure 5b), indicating that there was an obvious interaction between the host **8OA-N** and the guest C_{60}.[40] In the UV−vis and fluorescence emission spectra (Figures 5c and d, S29, and S30), we can see the fluorescence was distinctly quenched after the addition of C_{60}. This phenomenon is same as that in previous reports and indicates that these naphthalene-oxacalix[*m*]arene[*n*]pyrimidines interact strongly with fullerene C_{60}.[41] We tried to use C_{60} as the supramolecular guest template to grow the crystals. However, a dark red needle solid was obtained after many attempts, and we failed to get good crystals for the collection of X-ray diffraction data. Regardless, the unique concave cavity structure of **4OA-N**, **6OA-N**, and **8OA-N** can construct supramolecular systems with C_{60} by noncovalent bonds.

Electrochemical Studies: Cyclic Voltammograms and the Gibbs Free Energy Changes of the Photoinduced Electron Transfer (PET). The redox properties of the dyads were studied by cyclic voltammetry (Figure 6 and Table 3). **4OA-N** exhibited irreversible oxidation waves at +1.39 (in DCM) and +0.42 V (in ACN) and irreversible reduction waves at −1.02 (in DCM) and −2.40 V (in ACN). From the redox potentials as described above, the free energy ($\triangle G_{CS}$) of PET was calculated using the Weller equation (eqs 4−6).[42] The values of ΔG_{CS} are negative in all solutions and become more negative as the solution polarity increases. This result suggests that charge separation (CS) can also occur in *n*-hexane.

https://doi.org/10.1021/acsomega.1c07068
ACS Omega 2022, 7, 15411−15422

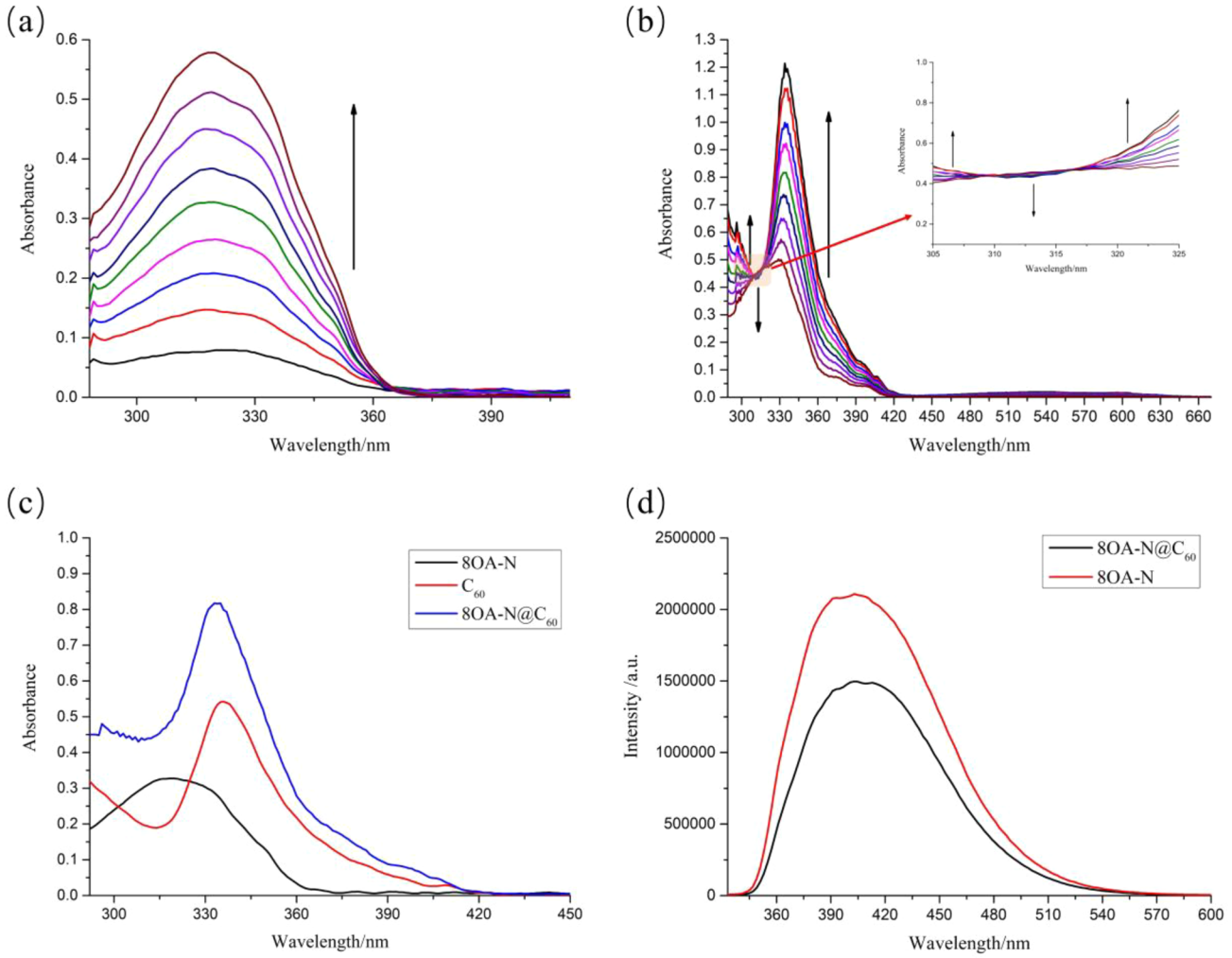

Figure 5. (a) UV−vis absorption spectra of different concentrations of **8OA-N** in toluene at 25 °C. The concentrations of **8OA-N** (from bottom to top) are 2.13×10^{-6}, 4.27×10^{-6}, 6.40×10^{-6}, 8.53×10^{-6}, 10.67×10^{-6}, 12.80×10^{-6}, 14.93×10^{-6}, 17.07×10^{-6}, and 19.20×10^{-6} M. (b) UV−vis absorption spectra of **8OA-N** in toluene the presence of different concentrations of C_{60} at 25 °C. The concentrations of C_{60} (from bottom to top) are 2.13×10^{-6}, 4.27×10^{-6}, 6.40×10^{-6}, 8.53×10^{-6}, 10.67×10^{-6}, 12.80×10^{-6}, 14.93×10^{-6}, 17.07×10^{-6}, 19.20×10^{-6} M. (c) UV−vis absorption spectra of **8OA-N**, **8OA-N@C_{60}**, and C_{60}. (d) Emission spectra **8OA-N** and **8OA-N@C_{60}** in toluene at 25 °C. The concentration of **8OA-N** and C_{60} is 1.1×10^{-5} M.

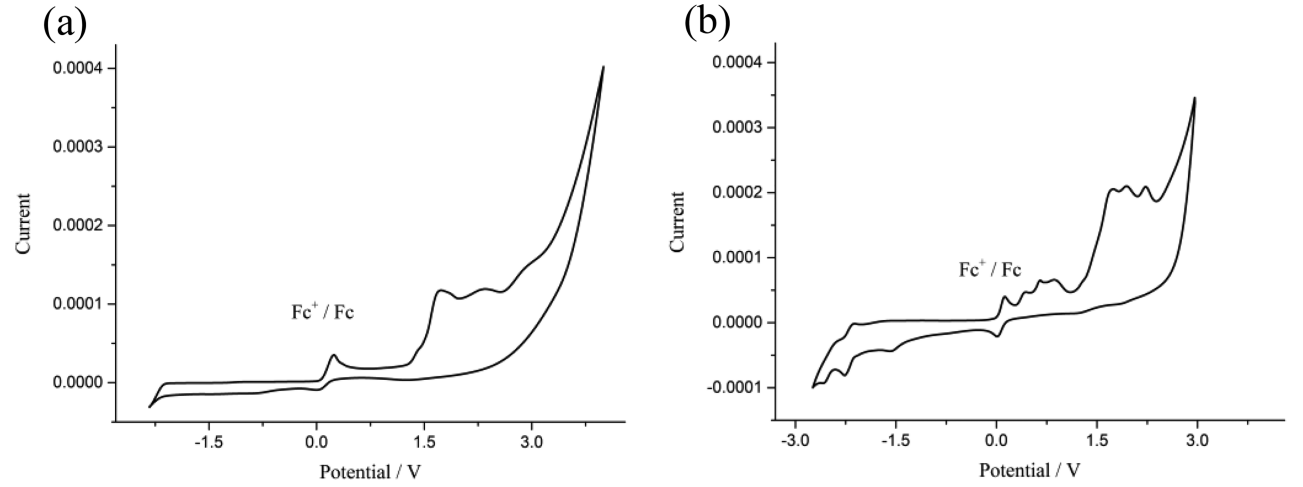

Figure 6. Cyclic voltammograms of **4OA-N** in (a) deaerated DCM and (b) deaerated ACN. Ferrocene (Fc) was used as the internal reference (set as 0 V in the cyclic voltammograms), and 0.10 M Bu_4NPF_6 was used as the supporting electrolyte. The scan rate was 100 mV s^{-1}, $c = 1.0 \times 10^{-3}$ M, and data were recorded at 20 °C.

https://doi.org/10.1021/acsomega.1c07068
ACS Omega 2022, 7, 15411−15422

Table 3. Electrochemical Redox Potentials,[a] Gibbs Free Energy Changes of the Charge Separation (ΔG_{CS}), and Charge-Separation-State Energy Levels (E_{CS}) of 4OA-N at 298 K

compd	E_{OX} (V)			E_{RED} (V)	
4OA-N	1.39			−1.02	
	0.42			−2.40	
	n-hexane	toluene	DCM	THF	ACN
$\triangle G_{CS}$ (eV)	−1.20	−1.32	−1.87	−1.83	−1.99
E_{CS} (eV)	2.42	2.24	1.72	1.76	1.58
$\triangle G_S$ (eV)	0.013	−0.17	−0.69	−0.65	−0.83

[a]Recorded with Bu_4NPF_6 as the electrolyte in CH_2Cl_2 (0.1 M) at room temperature. A Pt electrode was used as the counter electrode, a glassy carbon electrode was used as the working electrode, ferrocene (Fc/Fc^+) was used as the internal reference, and the $Ag/AgNO_3$ couple was used as the reference electrode.

Because $\triangle G_{CS}$ is less than 0, the intramolecular charge transfer (ICT) process is also present in solutions with different polarities, not just a single LE state.

$$\triangle G_s = -\frac{e^2}{4\pi\varepsilon_0 Rcc} - \frac{e^2}{8\pi\varepsilon_0}\left(\frac{1}{R_D} + \frac{1}{R_A}\right)\left(\frac{1}{\varepsilon_{REF}} - \frac{1}{\varepsilon_S}\right) \quad (4)$$

$$\triangle G_{CS} = e(E_{OX} - E_{RED}) - E_{00} + \triangle G_s \quad (5)$$

$$E_{CS} = e(E_{OX} - E_{RED}) + \triangle G_s \quad (6)$$

Nanosecond Transient Absorption Spectroscopy. To confirm the populations of the triplet excited states of the dyads upon photoexcitation, nanosecond time-resolved transient difference absorption spectroscopy was performed for **4OA-N** and **4OA-N@C_{60}**. For **4OA-N** (Figure 7a), the excited-state absorption (ESA) of the triplet state is the naphthalenen portion and the naphthalene-pyrimidine diplexes.[43] For **4OA-N@C_{60}** (Figure S31), ESA was observed not only for the host molecule but also for the guest molecule C_{60} in the range of 700−800 nm.[44] Interestingly, the triplet-state lifetime of **4OA-N** (τ_T = 35.7234 μs (0.57%), 7817.8111 μs (99.43%)) was longer than that of **4OA-N@C_{60}** (τ_T = 9.03 μs). We speculated that the triplet−triplet energy transfer (TTET) process occurred from **4OA-N** to C_{60}. Meanwhile, we calculated the attributions of the ESA bands (Figure S38) using time-dependent DFT (TD-DFT). For **4OA-N**, the ESA band at 385 nm is attributed to the $T_1 \rightarrow T_{28}$ transition, whereas the ESA band in the 450−550 nm region is attributed to $T_1 \rightarrow T_n$ (n = 8−19) transitions. Furthermore, the spin density of the triplet state is localized on the D−A moiety in **4OA-N** (Figure 7c), while that for **4OA-N@C_{60}** is localized on C_{60} (Figure 7d). This indicates that TTET occurred between the host and the guest.

DFT Calculations. The ground state (S_0) and the single excited state (S_1) of the complex were calculated with DFT and TD-DFT using the Gaussian 09 software package.[45−47] The ground-state frontier molecular orbitals of the compound are shown in Figure 8. The frontier molecular orbitals of the

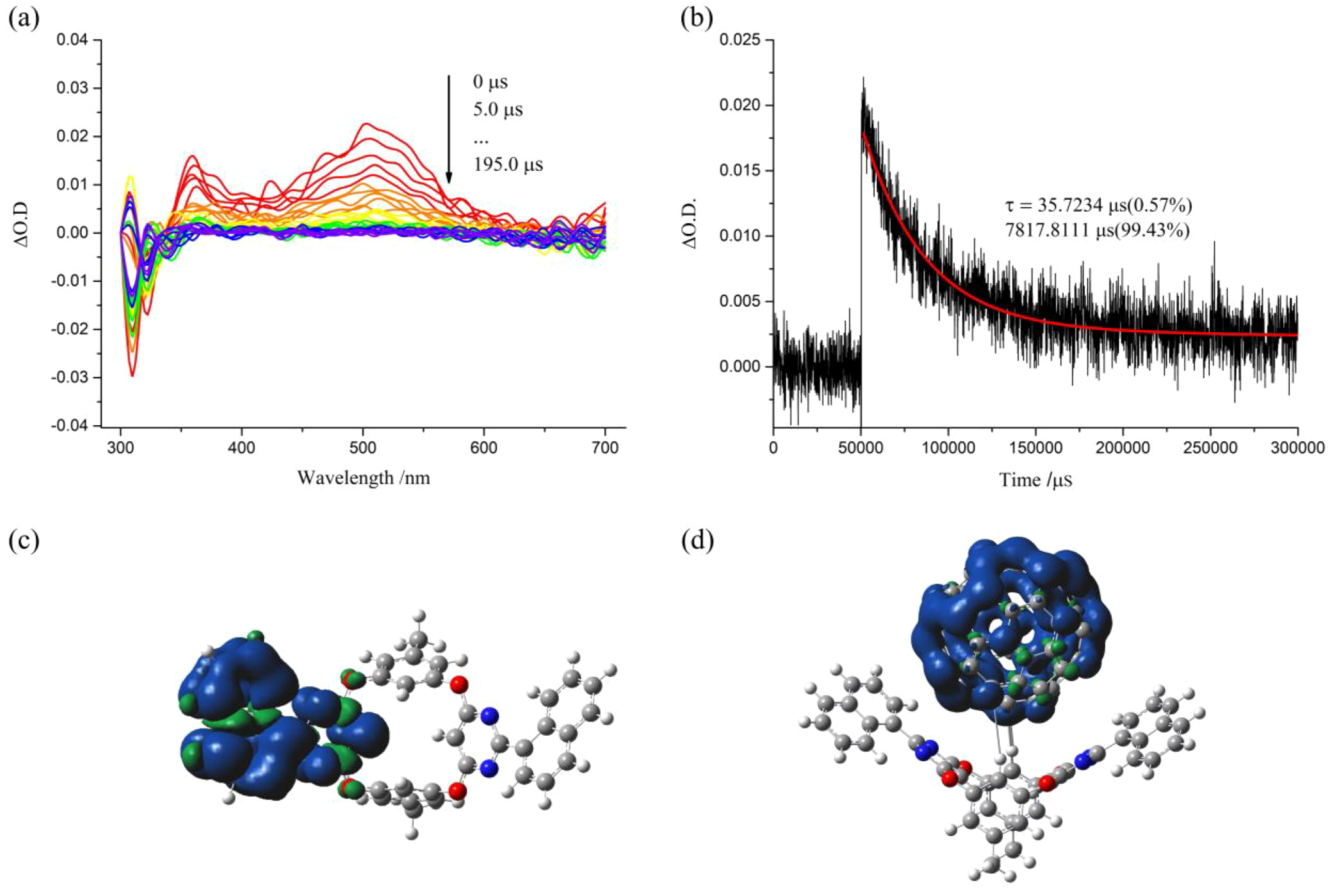

Figure 7. (a) Nanosecond transient absorption spectra of **4OA-N** (λ_{ex} = 350 nm) and (b) the τ_T values. Spin density surfaces of (c) **4OA-N** and (d) **4OA-N@C_{60}**.

https://doi.org/10.1021/acsomega.1c07068
ACS Omega 2022, 7, 15411−15422

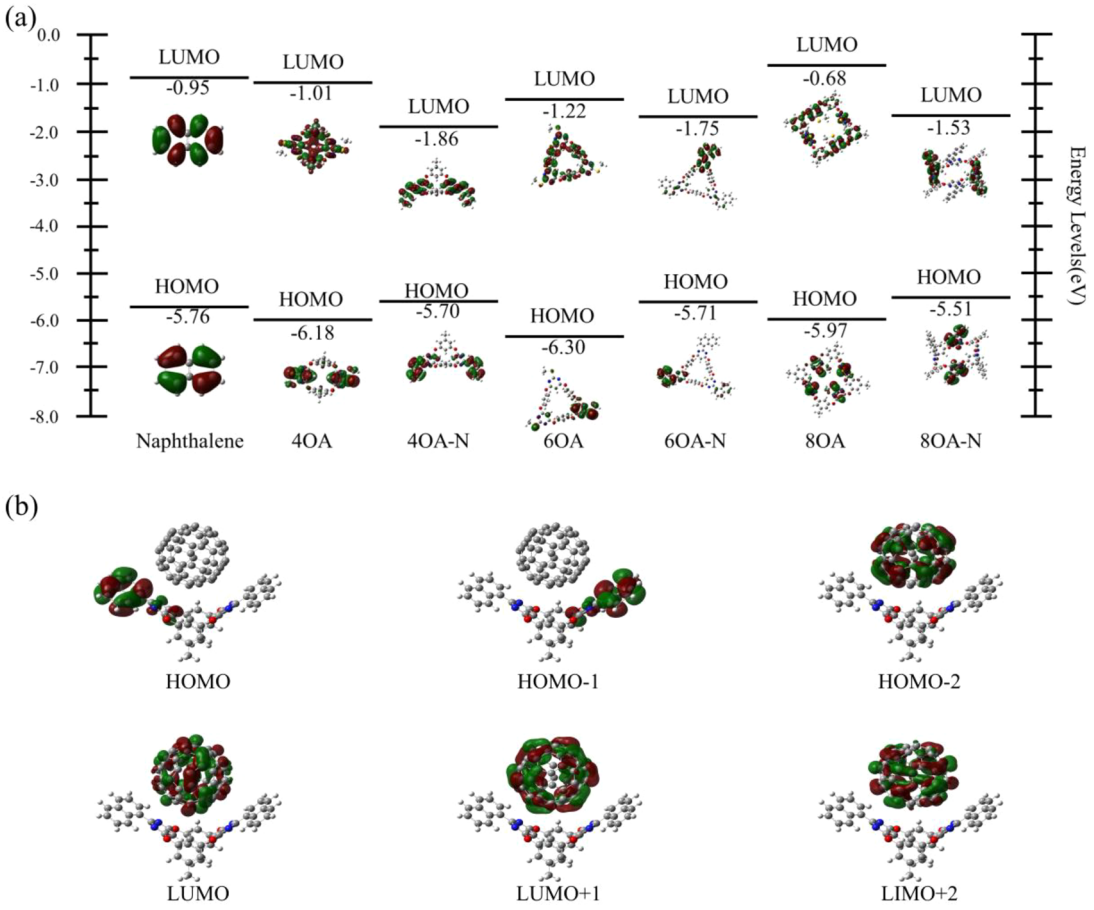

Figure 8. (a) Calculated HOMO and LUMO molecular ground-state orbitals of naphthalene, **4OA**, **6OA**, **8OA**, **4OA-N**, **6OA-N**, and **8OA-N**. (b) Ground-state frontier molecular orbital distribution of **4OA-N@C_{60}**.

Table 4. The UV−vis Absorption and Singlet-State (Fluorescence) Energy (Calculated at TDDFT/B3LYP/6-31G(d)) of 4OA-N, 6OA-N, and 8OA-N

		TDDFT/B3LYP/6-31G(d)				
compd	electronic transition[a]	excitation energy		f[b]	composition[c]	CI[d]
4OA-N	UV−vis	$S_0 \rightarrow S_1$	3.5106 eV (353 nm)	0.6747	H − 1 → L	0.5453
		$S_0 \rightarrow S_2$	3.5408 eV (350 nm)	0.3069	H → L	0.5586
	fluorescence	$S_0 \rightarrow S_1$	3.1307 eV (396 nm)	0.5233	H → L	0.7003
		$S_0 \rightarrow S_3$	3.6922 eV (336 nm)	0.4350	H − 1 → L + 1	0.6970
6OA-N	UV−vis	$S_0 \rightarrow S_1$	3.5734 eV (347 nm)	0.6463	H − 2 → L	0.5161
		$S_0 \rightarrow S_2$	3.5810 eV (346 nm)	0.7485	H → L + 2	0.4200
	fluorescence	$S_0 \rightarrow S_1$	3.1064 eV (399 nm)	0.5404	H → L	0.7000
		$S_0 \rightarrow S_4$	3.6480 eV (340 nm)	0.6938	H − 1 → L + 1	0.4582
8OA-N	UV−vis	$S_0 \rightarrow S_1$	3.6329 eV (341 nm)	0.0000	H− 1 → L + 2	0.4167
		$S_0 \rightarrow S_2$	3.6418 eV (340 nm)	0.2600	H → L + 2	0.3737
	fluorescence	$S_0 \rightarrow S_1$	3.1192 eV (397 nm)	0.3091	H → L	0.6997
		$S_0 \rightarrow S_2$	3.3525 eV (370 nm)	0.0004	H − 3 → L	0.7021

[a]Only selected excited states were considered. Numbers in parentheses are the excitation energy in wavelength. [b]Oscillator strength. [c]H stands for the HOMO and L stands for the LUMO. Only the main configurations are presented. [d]Coefficient of the wave function for each excitation. CI coefficients are given in absolute values.

HOMO in **8OA** (Figure S34a) are localized on the pyrimidine part, and those of the LUMO are distributed on the whole molecule. This means that the molecular orbitals of pyrimidine and benzene in **8OA** are separated from each other. Considering its symmetry and large pore size, both the HOMO and the LUMO in **8OA-N** (Figure S34b) are distributed over two opposite naphthalene and pyrimidine units. Different from **8OA**, the **8OA-N** molecular orbitals overlap each other. The result is further illustrated in Figure 8a. The HOMO − LUMO gap ($\triangle E$) is 4.81 eV for naphthalene and 5.29 eV for **8OA** in their ground states, while the $\triangle E$ of **8OA-N** is 3.98 eV. This indicates that the reduction of $\triangle E$ is due to the overlap of the **8OA-N** molecular orbitals. The same

https://doi.org/10.1021/acsomega.1c07068
ACS Omega 2022, 7, 15411−15422

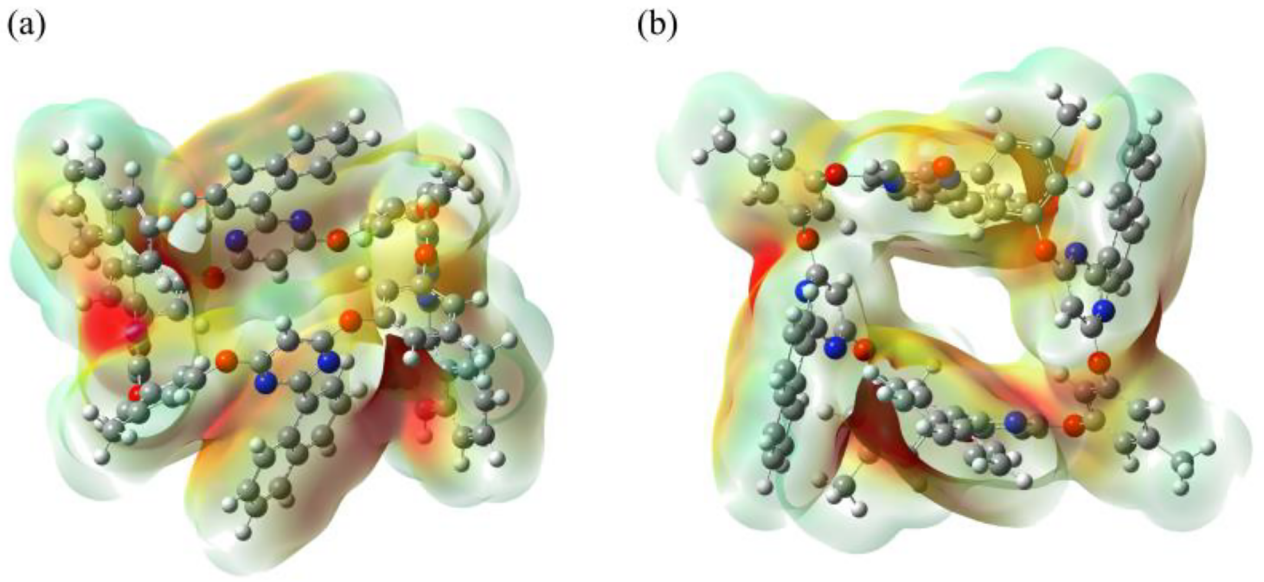

Figure 9. (a) Inner view and (b) outer view of the electrostatic potential mapped onto the electron density isosurface of **8OA-N** (red represents deficient electrons and blue represents rich electrons).

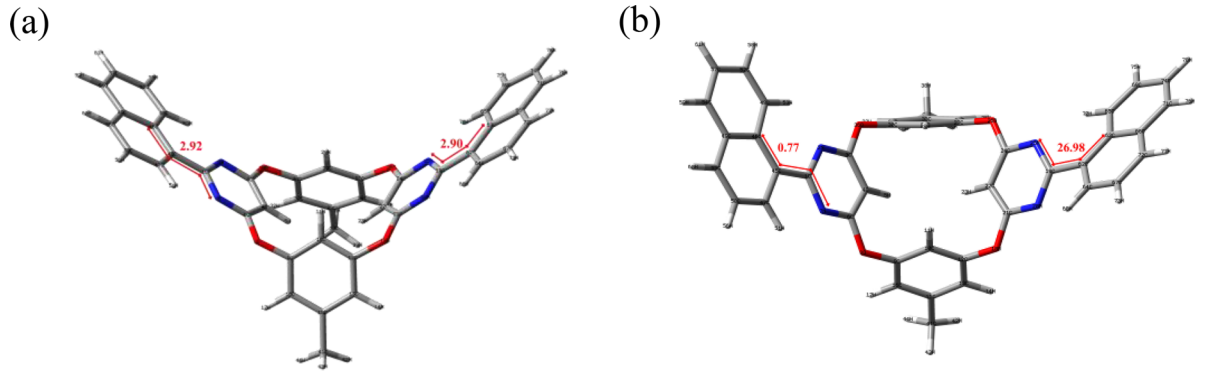

Figure 10. Dihedral angle of of **4OA-N** in (a) the ground state and (b) the excited state. Calculations were performed at the B3LYP/6-31G(d) level with Gaussian 09W.

conclusion was reached for **4OA**, **4OA-N**, **6OA**, and **6OA-N** (Figure S32 and S33).

Meanwhile, we calculated the molecular orbital distribution of the **4OA-N@C_{60}** supramolecular system (Figure 8b). Because the LUMO energy level of C_{60} is lower than that of the host molecule, the HOMO of **4OA-N@C_{60}** is distributed on **4OA-N** and the LUMO is localized on fullerene C_{60}. This indicates that the host−guest molecular orbitals in supramolecular systems are separated from each other, which is consistent with experimental results showing that the UV−vis absorption peak of the host molecule changed to C_{60} after the construction of the **4OA-N@C_{60}** supramolecular system.

From the theoretical calculation of the UV−vis absorption spectrum (Figure S37a and Table 4), we can see that the $S_0 \rightarrow S_1$ transition in **8OA-N** is symmetrically forbidden and the absorption is mainly derived from HOMO − LUMO + 2 ($S_0 \rightarrow S_2$ electronic transition), which leads to the decrease of the **8OA-N** quantum yield and explains why it is lower than the other molecules (Table 1). Compared with **4OA-N** and **6OA-N**, the distorted conformation of **8OA-N** may cause the decrease of the fluorescence quantum yield. The distorted conformation also impacts the binding of host and guest because the complexation constant of **8OA-N** is also the lowest (Table 2). The fluorescence calculations of **4OA-N**, **6OA-N**, and **8OA-N** reveal that the $S_0 \rightarrow S_1$ electronic transition is mainly derived from HOMO − LUMO and partly overlapped, which indicates that the lowest excited transition state is a LE state. The result of the theoretical calculations is in agreement with the experimental results (Figures S35−S37 and S39−S41).

At the ground and excited states of the electrostatic potential (ESP) of **4OA-N**, **6OA-N**, and **8OA-N** (Figures 9a and b, S42, and S43), the electron-deficient portions of the three compounds are concentrated on the pyrimidine and bridging oxygen atoms and can interact with fullerene C_{60}. Moreover, the electron-rich methyl group can also form a C−H···π interaction with C_{60}. This ESP result also further confirms that naphthalene-oxacalix[m]arenes are suitable "nests" for fullerene C_{60}.

Interestingly, taking **4OA-N** as an example (Figures 10, S44, and S45), the dihedral angle between naphthlene and pyrimidine is about 3° at the ground state, which is smaller than that in the excited state (near 27°). According to previous studies, an orthogonal geometry is beneficial for spin−orbit charge-transfer intersystem crossing (SOCT-ISC).[48] These different dihedral angles between the π-conjugation planes may

https://doi.org/10.1021/acsomega.1c07068
ACS Omega 2022, 7, 15411−15422

contribute to the different ISC efficiencies of the compounds, although it is difficult to confirm this issue explicitly; in other words, a few factors may simultaneously contribute to the SOCT-ISC efficiency. The other two dyads show higher singlet oxygen quantum yields than **4OA-N** (Table 2), which is attributed to them having more D−A units.

CONCLUSION

In summary, novel oxacalix[*m*]arene[*n*]pyrimidine derivatives decorated with luminescent-emission naphthyl groups were prepared through a cross-coupling reaction. The structure of naphthlene-oxacalix[*m*]arene[*n*]pyrimidine (**8OA-N**) was confirmed by single-crystal analysis. Photoluminescence (PL) spectra and electrochemical studies certified that the emission belongs to the LE state and exhibits the PET process. Meanwhile, nanosecond transient absorption spectra and the spin density of the compounds indicate that the triplet lifetime of **4OA-N** (τ_T = 35.7234 (0.57%), 7817.8111 μs (99.43%)) is longer than that of the supramolecular system (**4OA-N@C$_{60}$**, τ_T = 9.03 μs), which may be due to the TTET between the host and the guest. Dihedral angle optimization suggests that the degree of torsion between the donor and the acceptor promotes the ISC. The result of theoretical calculations is in good agreement with the experimental results. Contrary to previous reports that oxacalix[*m*]arene[*n*]pyrimidine could not recognize fullerene C_{60} very well, these naphthalene-oxacalix[*m*]arenes can form stable 1:1 host−guest complexes, and complexation constants from 4.10×10^4 to 6.68×10^4 M^{-1} were determined through fluorescence titration. These oxacalix[*m*]arene[*n*]pyrimidines with suitable pore sizes and concave conformations are potent "hunters" of fullerene (C_{60}). The fluorescence emission is obviously quenched by the addition of fullerene C_{60}, which means there is CT between the host oxacalix[*m*]arene and the fullerene guest. The strength of complexation is related not only to the pore size but also the molecular configuration. The experimental results were also verified through theoretical calculations, showing us that oxacalix[*m*]arene[*n*]pyrimidine can recognize fullerene C_{60} well. Taking into account that the oxacalix[*m*]arene[*n*]-pyrimidines are easy to modify chemically, versatile oxacalix-[*m*]arene derivatives could be synthesized by reasonable design and applied in supramolecular chemistry.

ASSOCIATED CONTENT

Supporting Information

The Supporting Information is available free of charge at https://pubs.acs.org/doi/10.1021/acsomega.1c07068.

Materials and methods; synthesis details; crystallographic data; 1H NMR, UV−vis, fluorescence, and nanosecond transient absorption spectra; Job's plots; and DFT calculations (PDF)

AUTHOR INFORMATION

Corresponding Authors

Yuming Yu − *State Key Laboratory of Chemistry and Utilization of Carbon-Based Energy Resources, College of Chemistry, Xinjiang University, Urumqi, Xinjiang 830017, P. R. China*; Email: yym2009@iccas.ac.cn

Zhenjiang Liang − *Pneumology Department, Shenzhen Children's Hospital, Shenzhen, Guangdong 518026, China*; Email: 552081911@qq.com

Hui Tan − *Pneumology Department, Shenzhen Children's Hospital, Shenzhen, Guangdong 518026, China*; Email: huitan@email.szu.edu.cn

Authors

Wei Lan − *State Key Laboratory of Chemistry and Utilization of Carbon-Based Energy Resources, College of Chemistry, Xinjiang University, Urumqi, Xinjiang 830017, P. R. China*; orcid.org/0000-0003-1825-2823

Xin Wang − *State Key Laboratory of Chemistry and Utilization of Carbon-Based Energy Resources, College of Chemistry, Xinjiang University, Urumqi, Xinjiang 830017, P. R. China*

Ming Gao − *State Key Laboratory of Chemistry and Utilization of Carbon-Based Energy Resources, College of Chemistry, Xinjiang University, Urumqi, Xinjiang 830017, P. R. China*

Rongrong Yang − *State Key Laboratory of Chemistry and Utilization of Carbon-Based Energy Resources, College of Chemistry, Xinjiang University, Urumqi, Xinjiang 830017, P. R. China*

Dou Wang − *State Key Laboratory of Chemistry and Utilization of Carbon-Based Energy Resources, College of Chemistry, Xinjiang University, Urumqi, Xinjiang 830017, P. R. China*

Shijun Sun − *State Key Laboratory of Chemistry and Utilization of Carbon-Based Energy Resources, College of Chemistry, Xinjiang University, Urumqi, Xinjiang 830017, P. R. China*

Yiran Wu − *State Key Laboratory of Chemistry and Utilization of Carbon-Based Energy Resources, College of Chemistry, Xinjiang University, Urumqi, Xinjiang 830017, P. R. China*

Yanfang Ma − *State Key Laboratory of Chemistry and Utilization of Carbon-Based Energy Resources, College of Chemistry, Xinjiang University, Urumqi, Xinjiang 830017, P. R. China*

Islam Siraj − *State Key Laboratory of Chemistry and Utilization of Carbon-Based Energy Resources, College of Chemistry, Xinjiang University, Urumqi, Xinjiang 830017, P. R. China*

Lang Liu − *State Key Laboratory of Chemistry and Utilization of Carbon-Based Energy Resources, College of Chemistry, Xinjiang University, Urumqi, Xinjiang 830017, P. R. China*; orcid.org/0000-0002-2390-8738

Duo-zhi Wang − *State Key Laboratory of Chemistry and Utilization of Carbon-Based Energy Resources, College of Chemistry, Xinjiang University, Urumqi, Xinjiang 830017, P. R. China*

Jianzhang Zhao − *State Key Laboratory of Chemistry and Utilization of Carbon-Based Energy Resources, College of Chemistry, Xinjiang University, Urumqi, Xinjiang 830017, P. R. China; State Key Laboratory of Fine Chemicals, School of Chemical Engineering, Dalian University of Technology, Dalian, Liaoning 116024, P. R. China*

Xiaodong Cai − *Department of Neurosurgery, The First Affiliated Hospital of Shenzhen University, Shenzhen Second People's Hospital, Shenzhen, Guangdong 518026, China*

Complete contact information is available at: https://pubs.acs.org/10.1021/acsomega.1c07068

Notes

The authors declare no competing financial interest.

https://doi.org/10.1021/acsomega.1c07068
ACS Omega 2022, 7, 15411−15422

■ ACKNOWLEDGMENTS

We thank Prof. Jianzhang Zhao (State Key Laboratory of Fine Chemicals, Dalian University of Technology) for support with the theoretical calculations and spectral testing. We also thank the National Natural Science Foundation of China (nos. 21861038 and 21961040), Supported by 111 Project (D18022), the Scientific Research Program of the Higher Education Institution of Xinjiang (no. XJEDU2018Y015), the Shenzhen Science and Technology Innovation Commission (nos. JCYJ20180507183036060, JCYJ20180228162928828, and ZDSYS20200811142600003), the Shanghai Cooperation Organization Science and Technology Partnership Program (no. 2021E01014), and the State Key Laboratory of Fine Chemicals at Dalian University of Technology (KF1903) for financial support.

■ REFERENCES

(1) Wang, M. X.; Zhang, X. H.; Zheng, Q. Y. Synthesis, structure, and [60] fullerene complexation properties of azacalix [m] arene [n] pyridines. *Angew. Chem. Int. Edit* **2004**, *43*, 838−842.
(2) Hudson, R.; Katz, J. L. Oxacalixarenes. In *Calixarenes and Beyond*; Neri, P.; Sessler, J. L.; Wang, M.-X., Eds.; Springer International Publishing: Cham, The Netherlands, 2016; pp 399−420.
(3) Shinkai, S. Calixarenes-the third generation of supramolecules. *Tetrahedron* **1993**, *49*, 8933−8968.
(4) Mascal, M.; Armstrong, A.; Bartberger, M. D. Anion− aromatic bonding: a case for anion recognition by π-acidic rings. *J. Am. Chem. Soc.* **2002**, *124*, 6274−6276.
(5) Alkorta, I.; Rozas, I.; Elguero, J. Interaction of anions with perfluoro aromatic compounds. *J. Am. Chem. Soc.* **2002**, *124*, 8593−8598.
(6) Wu, J.; Zhao, L.; Wang, D.; Wang, M. Synthesis, Structure and Coordination Self-Assembly of Azacalix [4-n] pyridine [n] pyrazines (n= 1−3). *Chin. J. Chem.* **2013**, *31*, 589−597.
(7) Quiñonero, D.; Garau, C.; Rotger, C.; Frontera, A.; Ballester, P.; Costa, A.; Deyà, P. M. (2002). Anion−π interactions: do they exist ? *Angew. Chem. Int. Edit* **2002**, *41*, 3389−3392.
(8) Zou, F.; Wu, B. P.; Wang, X. X.; Chen, Y. Y.; Koh, K.; Wang, K. M.; Chen, H. X. Signalamplification and dual recognition strategy for small-molecule detection by surface plasmon resonance based on calix [4] arene crown ether-modified gold nanoparticles. *Sens. Actuators, B* **2017**, *241*, 160−167.
(9) Matsumiya, H.; Masai, H.; Terazono, Y.; Iki, N.; Miyano, S. Chelating adsorbent for heavy metal ions prepared by loading anion-exchange resin with thiacalix [4] arenetetrasulfonate. *Bull. Chem. Soc. Jpn.* **2003**, *76*, 133−136.
(10) Nazeeruddin, M. K.; Pechy, P.; Grätzel, M. Efficient panchromatic sensitization of nanocrystallineTiO2 films by a black dye based on atrithiocyanato−ruthenium complex[J]. *Chem. Commun.* **1997**, *18*, 1705−1706.
(11) Ito, A.; Ono, Y.; Tanaka, K. Tetraaza [1. 1. 1.1] metacyclophane. *New J. Chem.* **1998**, *22*, 779−781.
(12) Maes, W.; Dehaen, W. Oxacalix [n](het) arenes. *Chem. Soc. Rev.* **2008**, *37*, 2393−2402.
(13) Van Rossom, W.; Robeyns, K.; Ovaere, M.; Van Meervelt, L.; Dehaen, W.; Maes, W. Odd- numbered oxacalix[*n*] arenes (*n* = 5, 7): Synthesis and solid-state structures. *Org. Lett.* **2011**, *13*, 126−129.
(14) Zhu, Y. P.; Yuan, J. J.; Li, Y. T.; Gao, M.; Cao, L. P.; Ding, J. Y.; Wu, A. X. One-Pot Synthesis of Oxacalixarene Derivatives with Tunable Cavity Size Using Miscellaneous Linkers. *Synlett* **2011**, *2011*, 52−56.
(15) Van Rossom, W.; Caers, J.; Robeyns, K.; Van Meervelt, L.; Maes, W.; Dehaen, W. (Thio)ureido anion receptors based on a 1, 3-alternate oxacalix [2] arene [2] pyrimidine scaffold. *J. Org. Chem.* **2012**, *77*, 2791−2797.
(16) Hu, S. Z.; Chen, C. F. Triptycene-derived oxacalixarene with expanded cavity: synthesis, structure and its complexation with fullerenes C 60 and C 70. *Chem. Commun.* **2010**, *46*, 4199−4201.
(17) Kroto, H. W.; Heath, J. R.; O'Brien, S. C.; Curl, R. F.; Smalley, R. E. C60: buckminsterfullerene. *Nature* **1985**, *318*, 162−163.
(18) Raffaini, G.; Citterio, A.; Galimberti, M.; Catauro, M. A Molecular Dynamics Study of Noncovalent Interactions between Rubber and Fullerenes. *Macromol. Symp.* **2021**, *395*, 2000198.
(19) Otieno, F.; Kotane, L.; Airo, M.; Billing, C.; Erasmus, R. M.; Wamwangi, D.; Billing, D. G. Probing the properties of polymer/non-fullerene/fullerene bulk heterojunction ternary blend solar cells, study of varied blend ratios of PBDB-T:ITIC-Th:PC 71 BM. *Eur. Phys. J. Plus* **2021**, *136*, 171.
(20) Sergeyev, D.; Ashikov, N.; Zhanturina, N. Electric Transport Properties of a Model Nanojunction "Graphene−Fullerene C_{60}− Graphene. *Int. J. Nanosci* **2021**, *20*, 2150007.
(21) Fa, S. X.; Wang, L. X.; Wang, D. X.; Zhao, L.; Wang, M. X. Synthesis, structure, and fullerene-complexing property of azacalix [6] aromatics. *J. Org. Chem.* **2014**, *79*, 3559−3571.
(22) Li, M. J.; Huang, C. H.; Lai, C. C.; Chiu, S. H. Hemicarceplex formation with a cyclotriveratrylene-based molecular cage allows isolation of high-purity ($\geq$ 99.0%) C_{70} directly from fullerene extracts. *Org. Lett.* **2012**, *14*, 6146−6149.
(23) Yanagisawa, M.; Tashiro, K.; Yamasaki, M.; Aida, T. Hosting fullerenes by dynamic bond formation with an iridium porphyrin cyclic dimer: a "chemical friction" for rotary guest motions. *J. Am. Chem. Soc.* **2007**, *129*, 11912−11913.
(24) Inokuma, Y.; Arai, T.; Fujita, M. Networked molecular cages as crystalline sponges for fullerenes and other guests. *Nat. Chem.* **2010**, *2*, 780−783.
(25) Wu, J. C.; Wang, D. X.; Huang, Z. T.; Wang, M. X. A [2+ 3] fragment coupling approach to N, O-bridged calix [1] arene [4] pyridines and their complexation with C_{60}. *Tetrahedron Lett.* **2009**, *50*, 7209−7212.
(26) Rossom, W. V.; Kundrát, O.; Ngo, T. H.; Lhoták, P.; Dehaen, W.; Maes, W. An oxacalix [2] arene [2] pyrimidine-bis (Zn-porphyrin) tweezer as a selective receptor towards fullerene C_{70}. *Tetrahedron Lett.* **2010**, *51*, 2423−2426.
(27) Van Rossom, W.; Maes, W.; Kishore, L.; Ovaere, M.; Van Meervelt, L.; Dehaen, W. Efficient post-macrocyclization functionalizations of oxacalix [2] arene [2] pyrimidines. *Org. Lett.* **2008**, *10*, 585−588.
(28) Maes, W.; Van Rossom, W.; Van Hecke, K.; Van Meervelt, L.; Dehaen, W. Selective synthesis of functionalized thia-and oxacalix [2] arene [2] pyrimidines. *Org. Lett.* **2006**, *8*, 4161−4164.
(29) Liebeskind, L. S.; Srogl, J. Thiol ester− boronic acid coupling. A mechanistically unprecedented and general ketone synthesis. *J. Am. Chem. Soc.* **2000**, *122*, 11260−11261.
(30) Prokopcova, H.; Kappe, C. O. The Liebeskind−Srogl C-C Cross-Coupling Reaction. *Angew. Chem. Int. Edit* **2009**, *48*, 2276−2286.
(31) Peng, L.; Xu, S.; Zheng, X.; Cheng, X.; Zhang, R.; Liu, J.; Liu, B.; Tong, A. Rational design of a red-emissive fluorophore with AIE and ESIPT characteristics and its application in light-up sensing of esterase. *Anal. Chem.* **2017**, *89*, 3162−3168.
(32) Kolandaivelu, S.; Rajamoni, J.; Kandasamy, S. NH···O, CH···O hydrogen-bonded supramolecular frameworks in 4-fluoroanilinium and dicyclohexylaminium picrate salts. *Struct Chem.* **2020**, *31*, 899−908.
(33) Grabowski, Z. R.; Rotkiewicz, K.; Rettig, W. Structural changes accompanying intramolecular electron transfer: focus on twisted intramolecular charge-transfer states and structures. *Chem. Rev.* **2003**, *103*, 3899−4032.
(34) Guo, R. K.; Kitamura, N.; Tazuke, S. Anomalous solvent effects on the twisted intramolecular charge transfer fluorescence of ethyl 4-(N, N-dimethylamino) benzoate in chlorinated solvents. *J. Phys. Chem.* **1990**, *94*, 1404−1408.
(35) Shan, H.; Liu, A.; Lv, Y.; Wu, X.; Ma, Y.; Jin, X.; Guo, J. Manipulating the AIE and low-temperature phosphorescence proper-

https://doi.org/10.1021/acsomega.1c07068
ACS Omega 2022, 7, 15411−15422

ties of o-carborane-imidazole derivatives via fine tuning their structural features. *Dyes Pigm* **2020**, *180*, 108400.
(36) Han, F.; Chi, L.; Wu, W.; Liang, X.; Fu, M.; Zhao, J. Environment sensitive phenothiazine dyes strongly fluorescence in protic solvents. *J. Photochem. Photobiol., A* **2008**, *196*, 10−23.
(37) Tang, X.; Bai, Q.; Peng, Q.; Gao, Y.; Li, J.; Liu, Y.; Yao, L.; Lu, P.; Yang, B.; Ma, Y. Efficient deep blue electroluminescence with an external quantum efficiency of 6.8% and CIE y< 0.08 based on a phenanthroimidazole−sulfone hybrid donor−acceptor molecule. *Chem. Mater.* **2015**, *27*, 7050−7057.
(38) Sutton, L. R.; Scheloske, M.; Pirner, K. S.; Hirsch, A.; Guldi, D. M.; Gisselbrecht, J. P. Unexpected Change in Charge Transfer Behavior in a Cobalt (II) Porphyrin− Fullerene Conjugate That Stabilizes Radical Ion Pair States. *J. Am. Chem. Soc.* **2004**, *126*, 10370−10381.
(39) Wang, J.; Wang, D.; Miller, E. K.; Moses, D.; Bazan, G. C.; Heeger, A. J. Photoluminescence of water-soluble conjugated polymers: Origin of enhanced quenching by charge transfer. *Macromolecules* **2000**, *33*, 5153−5158.
(40) Huerta, E.; Isla, H.; Pérez, E. M.; Bo, C.; Martín, N.; Mendoza, J. D. Tripodal exTTF-CTV hosts for fullerenes. *J. Am. Chem. Soc.* **2010**, *132*, 5351−5353.
(41) van Hal, P. A.; Knol, J.; Langeveld-Voss, B. M. W.; Meskers, S. C. J.; Hummelen, J. C.; Janssen, R. A. J. Photoinduced Energy and Electron Transfer in Fullerene− Oligothiophene− Fullerene Triads. *J. Phys. Chem. A* **2000**, *104*, 5974−5988.
(42) Shi, W. J.; El-Khouly, M. E.; Ohkubo, K.; Fukuzumi, S.; Ng, D. K. P. Photosynthetic Antenna-Reaction Center Mimicry with a Covalently Linked Monostyryl Boron-Dipyrromethene−Aza-Boron-Dipyrromethene−C_{60} Triad. *Chem. - Eur. J.* **2013**, *19*, 11332−11341.
(43) Pabst, M.; Lunkenheimer, B.; Köhn, A. A Model System for Triplet− Triplet Interactions and Its Spectral Properties. *J. Phys. Chem. C* **2011**, *115*, 8335−8344.
(44) Ziessel, R.; Allen, B. D.; Rewinska, D. B.; Harriman, A. Selective triplet-state formation during charge recombination in a fullerene/bodipy molecular dyad (Bodipy= Borondipyrromethene). *Chem. Eur. J.* **2009**, *15*, 7382−7393.
(45) Nishino, K.; Tanaka, K.; Chujo, Y. Tuning of Sensitivity in Thermochromic Luminescence by Regulating Molecular Rotation Based on Triphenylamine-Substituted o-Carboranes. *Asian J. Org. Chem.* **2019**, *8*, 2228−2232.
(46) Nishino, K.; Uemura, K.; Gon, M.; Tanaka, K.; Chujo, Y. Enhancement of aggregation-induced emission by introducing multiple o-carborane substitutions into triphenylamine. *Molecules* **2017**, *22*, 2009.
(47) Frisch, M.; Trucks, G.; Schlegel, H.; Scuseria, G.; Robb, M.; Cheeseman, J.; Scalmani, G.; Barone, V.; Mennucci, B.; Petersson, G.; Nakatsuji, H.; Caricatom, Li. X.; Hratchian, H.; Izmaylov, A.; Bloino, J.; Zheng, G.; Sonnenberg, J.; Hada, M.; Ehara, M.; Toyota, K.; Fukuda, R.; Hasegawa, J.; Ishida, M.; Nakajima, T.; Honda, Y.; Kitao, O.; Nakai, h.; Vreven, T.; Montgomery, J.; Peralta, J.; Ogliaro, F.; Bearpark, M.; Heyd, J.; Brothers, E.; Kudin, K.; Staroverov, V.; Kobayashi, R.; Normand, J.; Raghavachari, K.; Rendell, A.; Burant, J.; Iyengar, S.; Tomasi, J.; Cossi, M.; Rega, N.; Millam, J.; Klene, M.; Knox, J.; Cross, J.; Bakken, V.; Adamo, C.; Jaramillo, J.; Gomperts, R.; Stratmann, R.; Yazyev, O.; Austin, A.; Cammi, R.; Pomelli, C.; Ochterski, J.; Martin, R.; Morokuma, K.; Zakrzewski, V.; Voth, G.; Salvador, P.; Dannenberg, J.; Dapprich, S.; Daniels, A.; Farkas, Ö.; Foresman, J.; Ortiz, J.; Cioslowski, J.; Fox, D. *GAUSSIAN 09W*, rev. C.01; Gaussian, Inc., Wallingford, CT, 2009.
(48) Dance, Z. E. X.; Mickley, S. M.; Wilson, T. M.; Ricks, A. B.; Scott, A. M.; Ratner, M. A.; Wasielewski, M. R. Intersystem crossing mediated by photoinduced intramolecular charge transfer: julolidine−anthracene molecules with perpendicular π Systems. *J. Phys. Chem. A* **2008**, *112*, 4194−4201.

https://doi.org/10.1021/acsomega.1c07068
ACS Omega 2022, 7, 15411−15422